PENDING - Lender

GENERAL RECORD INFORMATION

Request Identifier:	**33223830**	**Status:**	PENDING 20070824
Request Date:	20070824	**Source:**	FSILLSTF
OCLC Number:	53832943		
Borrower:	GIE	**Need Before:**	20070831
Receive Date:		**Renewal Request:**	
Due Date:		**New Due Date:**	
Lenders:	*MWR, FER, FNN		
Request Type:	Copy		

AUG 2 ▪ 2007
SENT BY ARIEL

BIBLIOGRAPHIC INFORMATION

Call Number:	
Author:	Barnes, William L.
Title:	Earth observing systems VIII : 3-6 August, 2003, San Diego, California, USA /
ISBN:	9780819450241
Imprint:	Bellingham, Wash. : SPIE, 2003
Article:	Technique for estimating uncertainties in top-of-atmosphere radiances derived by vicarious calibration/Schiller, S.J.
Pages:	502–516
Verified:	WorldCat Desc: x, 634 p. : Type: Book

BORROWING INFORMATION

Patron:	G. Chander
Ship To:	U.S. Geological Survey-EROS/ATTN: Library/Mundt Federal Bldg./Sioux Falls, SD 57198-0001
Bill To:	same
Ship Via:	E-mail/fax preferred.
Electronic Delivery:	
Maximum Cost:	IFM - 20.00
Copyright Compliance:	CCL
Billing Notes:	IFM please; invoices not accepted. We do not charge. Thanks!
Fax:	605-594-2725
Email:	cdeering@usgs.gov
Affiliation:	FEDL, LVIS
Borrowing Notes:	Please send via e-mail to cdeering@usgs.gov.

LENDING INFORMATION

Lending Charges:

email GdE

Technique for estimating uncertainties in top-of-atmosphere radiances derived by vicarious calibration

Stephen J. Schiller*
Raytheon, Space and Airborne Systems Division, El Segundo, CA, USA 90245

ABSTRACT

Reflectance-based vicarious calibration of satellite sensors is a method by which in-situ radiometric measurements of a surface target and the atmosphere are used to constrain a radiative transfer model for estimating a top-of-atmosphere (TOA) radiance. The procedure provides an at-sensor radiance, independent of the on-board calibrator, that can be used to maintain knowledge of the in-flight calibration performance of the remote sensing system. However, an estimate of the TOA radiance is incomplete unless accompanied with an uncertainty that quantifies the random and systematic errors associated with that estimate. Presented in this paper is a methodology for predicting a TOA radiance with an absolute accuracy estimate derived using an error propagation analysis based principally on validation data recorded by calibrated ground-based radiometer measurements. A vicarious calibration data collect for the airborne sensor ATLAS and the IKONOS satellite on June 30, 2000 at Brookings, South Dakota provides a test case for this technique in the solar reflective spectrum. The results show that using a natural grass covered target under moderate aerosol loading, absolute accuracies between 3% and 5% are achieved for band integrated TOA radiances between 0.4 and 1.6 microns.

Keywords: Radiometry, Vicarious Calibration, Accuracy, IKONOS, ATLAS, MODTRAN

1. INTRODUCTION

For an orbiting remote sensing system designed to obtain quantitative measurements of the radiation scattered or emitted by a target source, developing techniques to maintain calibration through launch and to end-of-life is always a central issue. No matter how well designed an on-board calibration system may be, it is difficult to maintain the sensor calibration to the same level of accuracy in-flight as established prior to launch when characterized relative to standard sources in the laboratory environment. The harsh effects of launch and the extended exposure to vacuum related contamination processes can change the output of the calibration sources and the throughput of the sensor optical system in ways that may not be predictable in degradation models or detectable in the data sent to the ground.

To minimize the encroachment of unknown systematic errors methods have been developed to produce a known radiance at the entrance pupil of the orbiting sensor independent of the on-board calibrators. Such an approach is known as vicarious calibration, and one of the most widely used procedures is referred to as the reflectance-based technique[1,2,3]. By constraining a radiative transfer code with in-situ measurements of a target site at the time of the sensor overpass, the reflectance-based approach predicts the top-of-atmosphere (TOA) at-sensor radiance, thereby providing the data to obtain an independent measure of the sensor gain. The result can be compared to the gain derived from the on-board calibrator which allows as estimation of the accuracy of the in-flight image calibration process.

Inherent in the success of this effort is the need to have knowledge of the uncertainty in the vicariously predicted at-sensor radiance. The typical approach in deriving an uncertainty is to carry out a sensitivity analysis of the radiative transfer model and calculate a root-sum-square (RSS) error value. This would include estimates of all potentially significant error sources from the model and the calibration process influencing the determination of the band integrated TOA radiance. However, it may still be true that not all error sources are captured in such an analysis. There are bias errors from unmeasured and assumed model inputs, correlation errors between model parameters, and absolute errors in converting to physical units that may be unknown and unexplored. In addition, even "worst case" error estimates are generally chosen with high altitude desert playa targets in mind where critical characteristics for an ideal test site are

* Formerly at the address Physics Department, South Dakota State University, Brookings, South Dakota, 57007

Proceedings of SPIE Vol. 5151 Earth Observing Systems VIII, edited by William L. Barnes (SPIE, Bellingham, WA, 2003) · 0277-786X/2003/$15.00

consistently available. Characteristics such as high surface reflectance, spectral uniformity and low aerosol loading, that are typical of these sites, minimize atmospheric effects in the TOA signal[4].

What about the application of vicarious calibration at less ideal locations? As one starts dealing with environmental conditions that push the envelope in tuning a radiative transfer model to match the observed radiometric properties of the site, the need to estimate the TOA radiance uncertainty in a way that also assesses the model accuracy relative to site conditions becomes more critical. The approach presented in this paper attempts to do this. It is accomplished by first constraining the radiative transfer model with measurements of surface reflectance, atmospheric transmittance, and the diffuse-to-global ratio recorded at the time of the sensor overpass. Next, in-situ spectroradiometer observations of upwelling radiance off the target and sky path radiance are used to independently verify the model performance. Finally, once shown that the model output agrees with the radiance observations within measurement errors, indicating they are statistically equivalent, the uncertainties in the radiometer observations are integrated into a error propagation analysis of the TOA radiance. The result is an at-sensor radiance magnitude and absolute uncertainty estimate that intrinsically reflects the temporal radiometric quality of the target site. The approach provides a fairly rigorous estimate of the TOA radiance uncertainty in a way that explores all significant relative and bias error sources. Consequently, it should provide an uncertainty that the users of the vicarious calibration results will find reliable.

For nearly ideal playa targets, it is reported that uncertainties of 2 to 3% are achievable in predicting the TOA radiance[5,6,7,8]. The results of this investigation, for a less ideal location, show that when using a grass covered surface as the calibration target under stable sky conditions characterized by an extensive set of in-situ measurements, absolute uncertainties of 3% to 5% are obtainable for the solar reflective spectrum in the 0.4 to 1.6 micron range. This is demonstrated using the radiative transfer code MODTRAN 4[9] and in-situ data collected on June 30, 2000 at Brookings, SD in conjunction with the overflight of the ATLAS airborne sensor and the IKONOS satellite.

2. FIELD CAMPAIGN

The data for this investigation was collected as part of a field campaign carried out by South Dakota State University in collaboration with the NASA Stennis Space Center Earth Science Application Directorate. On June 30, 2000, a test site was characterized to provide the data for a vicarious calibration. Extensive ground truth data was recorded simultaneously with the overpass of a NASA Lear Jet flying ATLAS and the commercial satellite IKONOS, owned and operated by Space Imaging. This included measurements of surface reflectance and upwelling radiance, atmospheric transmittance, diffuse-to-global ratio of the hemispherical sky irradiance, and sky path radiance. A radiosonde vertical profile was also acquired close to the overpass times. The target area is shown in Figure 1 and consists of a grass covered field characterized over an area of 180 m by 180 m.

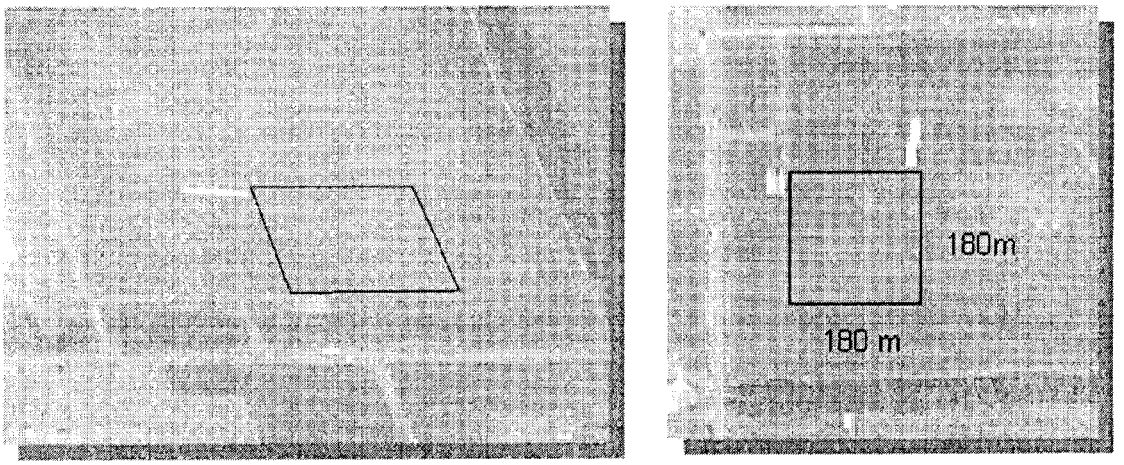

Figure 1. Pictures showing the vicarious calibration target recorded from the NASA Lear Jet flying ATLAS and from an IKONOS pan image. Blue tarps identify the North corners.

3. DATA FOR REFLECTANCE-BASED PREDICTION OF THE TOP-OF-ATMOSPHERE RADIANCE

The reflectance-based approach relies on measurements of the surface target reflectance and atmospheric optical properties coinciding with the sensor overpass. Both are used as input to the MODTRAN radiative transfer code, matching the model to environmental conditions. By setting the model path geometry to that of the downlooking sensor, the radiance reaching the sensor from the target is predicted. The following sections describe the field data collected to delimit the MODTRAN model.

3.1. Surface Reflectance

The reflectance of the target area was measured using an Analytical Spectral Devices FieldSpec® Full Range spectroradiometer (ASD). The ASD was walked across the field taking measurements along 6 north-south paths (separated by 30 meters) with individual spectra recorded every 10 m along the path. The field target was walked twice providing two separate data sets for the same target area, once between 11:00 and 11:25 Central Daylight Time (CDT) and a second time between 11:49 and 12:10 CDT.

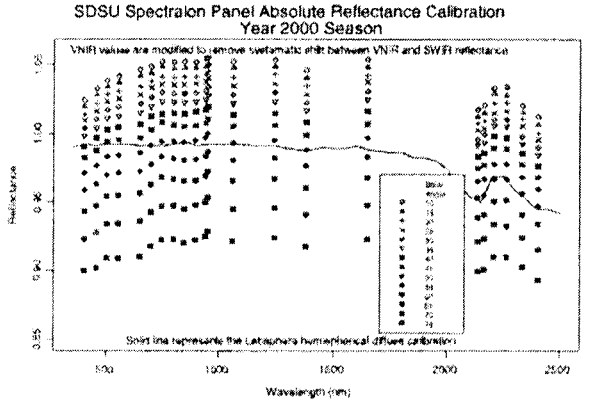

Figure 2. Bidirectional reflectance factor calibration for the SDSU Spectralon panel. The panel was calibrated at the University of Arizona Remote Sensing Group's Calibration Lab. The solid line is Labsphere's factory calibration (hemispherical reflectance) provided with the panel.

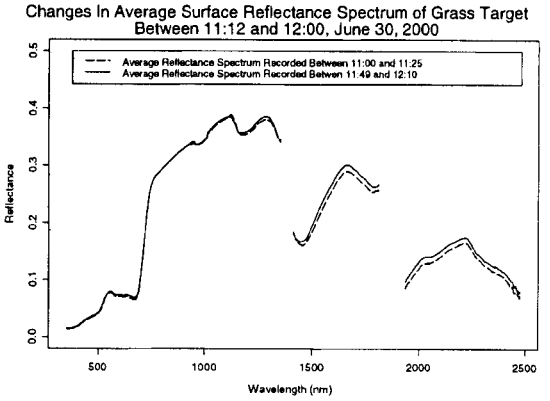

Figure 3. Average reflectance spectrum of the natural grass surface showing some bidirectional reflectance effects that appear in the shortwave infrared from the change solar zenith angle.

Over the site, 108 spectral files were recorded that sampled the 180 m by 180 m area uniformly in both collection events. Each spectrum was based on an average of 50 spectral scans. All the spectra for the two reflectance sets were averaged together to give the net reflectance spectrum of the entire target area. Reflectance panel spectra were recorded at the beginning, after each second row was walked, and at the end of the data collection period. The absolute reflectance of the panel as a function of solar zenith angle was obtained relative to a NIST reflectance standard providing an absolute reflectance reported to be accurate to better then 2%. Figures 2 and 3 show the reflectance calibration of the panel and the resulting average reflectance of the entire target area for the two collects. Using this calibration each raw radiance spectrum, recorded with the ASD of the grass surface target, was converted to reflectance that included a bidirectional reflectance factor correction for the solar zenith angle (Fig. 2) applied to each individual spectrum recorded.

3.2. Shadowband radiometer data

Sky conditions on June 30 were excellent. There was no cirrus visible with only a few small clouds forming in the afternoon. Shadowband radiometer observations for the entire day are presented in Figure 4, demonstrating the stable sky conditions that were present at the target site. These were obtained using a Yankee Environmental Systems Multi-Filter Rotating Shadowband Radiometer (MFRSR). An important observational data parameter obtained from the MFRSR is the diffuse-to-global ratio. This ratio is sensitive to solar geometry, surface reflectance of the surround (important to the adjacency effect), aerosol extinction and the scattering phase function. The ratio provides a characterization of the atmosphere in terms of a dimensionless quantity for input into MODTRAN. Constraining the model to match the observed diffuse-to-global ratio is accomplished by adjusting the asymmetry factor in the scattering phase function.

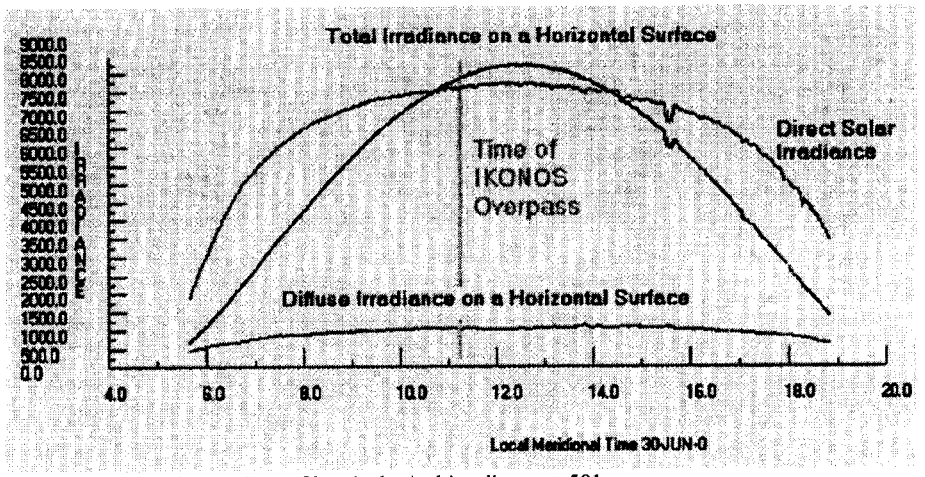

Figure 4. Shadowband radiometer observations of hemispherical irradiance at 501 nm.

3.3. Reagan solar radiometer observations

Atmospheric transmittance was monitored with an automated Reagan 10-channel solar radiometer. It recorded observations of direct solar irradiance in 1minute intervals from sunrise to sunset providing morning and afternoon Langley plots at nine wavelengths (10 nm bandwidths). It is from this data that extinction coefficients in the boundary layer are derived and used as input into MODTRAN. The following Langley plot shows the stability of the sky conditions throughout the morning on June 30.

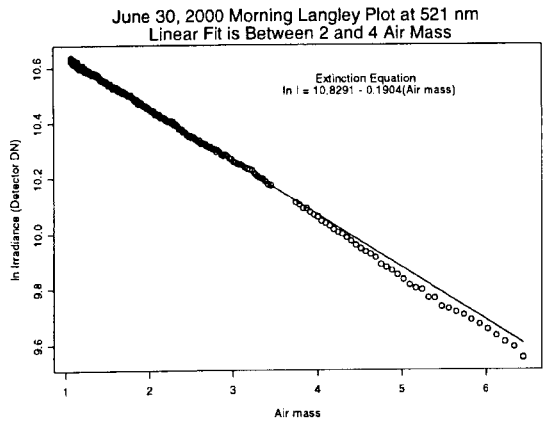

Figure 5. Morning Langely plot recorded by the Reagan solar radiometer at a nominal wavelength of 521 nm. The average extinction coefficient is 0.19.

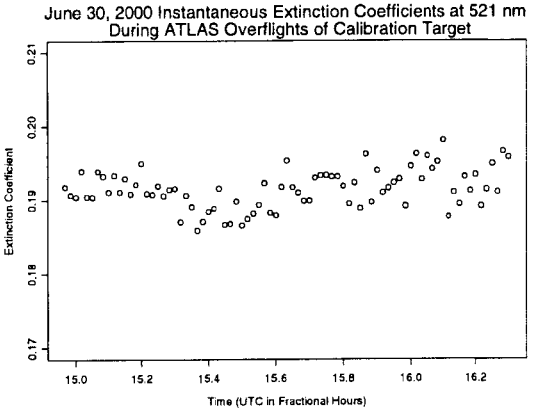

Figure 6. Instantaneous values of total atmospheric extinction recorded simultaneously with the reflectance data.

Instantaneous extinction coefficients derived from individual transmittance measurements are shown in Figure 6 maintaining an average value of 0.19. When aerosol loading is a minimum at the Brookings site, the extinction would be around 0.15. The instantaneous extinction is based on the seasonal average Langley plot calibration of the top-of-atmosphere irradiance signal, Io, obtained for each of the Reagan Channels. The seasonal calibration was carried out by determining Io from 45 Langley plots recorded over the summer of 2000. Corrections for changing sun/earth distance were included. The variability in Io from the seasonal analysis in presented in Table 2 and will be used to estimate the transmittance uncertainty in the TOA radiance error analysis.

4. PROCEDURE USED TO APPLY INPUTS TO MODTRAN

The diagram shown in Figure 7 summarizes a three step procedure that was followed to adjust the MODTRAN model to fit the measurements of transmittance, surface reflectance, and diffuse-to-global ratio presented in section 3. Once this procedure is completed MODTRAN is considered fully constrained by the in-situ measurements for predicting the TOA radiance. The following subsections illustrate the process using atmospheric data collected at the mid-time of the first reflectance collect between 11:00 and 11:25 CDT. It is done at this time to later validate the model (Sec. 4.2) by comparison to the ASD average target spectrum transformed to upwelling at-surface radiance based on an integrating sphere calibration.

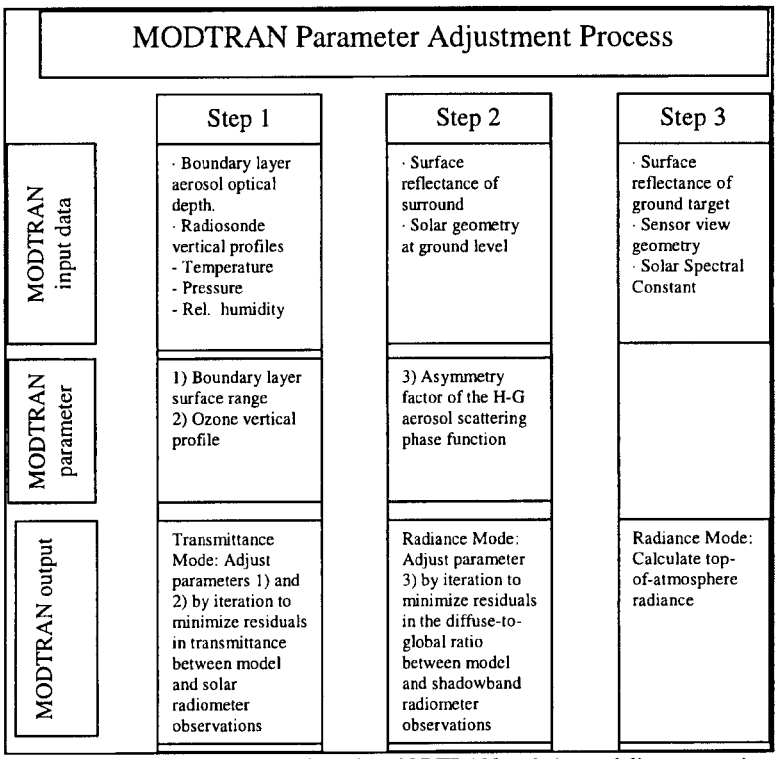

Figure 7. Three step procedure used to delimit the MODTRAN code in modeling target site conditions

4.1. Step 1:MODTRAN model fit to the total transmittance

In this step, MODTRAN is setup to form a two layer aerosol vertical profile based on the extinction coefficient, k, derived from solar radiometer observations of total transmittance. The solar air mass, m, was 1.223 and is used in the extinction law, $T=e^{-km}$, to convert the total transmittance to extinction values. The Rayleigh extinction is calculated, based on a ground level atmospheric pressure of 952 mb, and subtracted from the total extinction to give the total aerosol contribution. Finally, the upper atmosphere aerosol extinction above the boundary layer is subtracted from the total to give the results for the boundary layer. Table 1 presents the resulting boundary layer transmittance in the 5 Reagan channels unaffected by ozone.

Wavelength (nm)	Total transmittance at 11:13 CDT	Upper atmosphere aerosol extinction	Boundary layer aerosol extinction
380	0.5263	0.0276	0.0720
399	0.5910	0.0265	0.0549
441	0.6822	0.0248	0.0562
869	0.9506	0.0104	0.0164
1030	0.9520	0.0048	0.0281

Table 1. Extinction coefficients assigned to MODTRAN as a two layer aerosol vertical model

Though the analysis hinted that the aerosol size distribution may be bimodal, a single power law modeled by the Angstrom turbidity law is fit, by a least-squares regression, to these five points to obtain a smooth extrapolation to other wavelengths. The power law fit is then used to predict the boundary layer aerosol extinction at the standard MODTRAN input wavelengths which are normalized by dividing by the extinction at 550 nm and entered into card 2D2 for atmospheric layer 1. Twice during the summer of 2000, the Reagan solar radiometer was flown on an aircraft, under a cloudless sky, at the altitude MODTRAN internally assigns as the top of the boundary layer for the elevation of the Brookings site (~10,500 ft above sea level). The upper atmosphere transmittances from these two data sets were averaged and used to derive normalized extinction coefficients in the solar radiometer bands. The results were adopted as a seasonal value and placed in atmospheric layer 2. Aerosol extinction layers 3 and 4 were set to 0 so that total aerosol extinction to the top of the atmosphere was defined only by the observations.

Once the aerosol inputs are complete, MODTRAN is run in an iterative process adjusting the surface range in the boundary layer. The minimum residual fit to the observations was obtained using a surface range of 100 km and is plotted in Figure 8. It should be noted that absorption coefficients are used with values that correspond to a transmittance in which 5% of the light removed by extinction in the boundary layer is by absorption. At this point the ozone extinction can be fine tuned. This is typically done by scaling the 1976 standard atmosphere vertical profile to improve the model fit at 610 nm. However, the difference in the transmittance between the model and the observation was already within the uncertainty of the radiometer measurement at 610 nm (See Table 2) and was unchanged to avoid an artificial improvement to the error analysis.

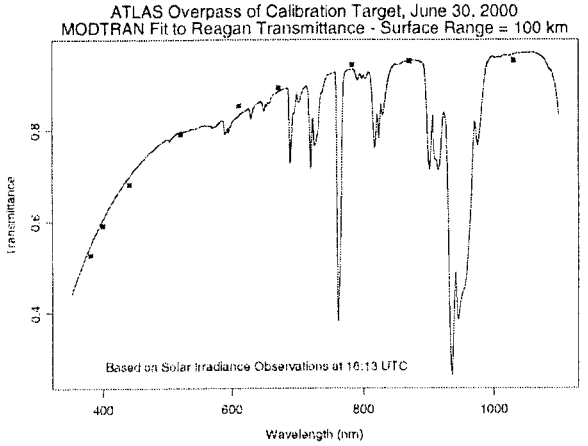

Figure 8. Final MODTRAN model fit tot the observed total transmittance.

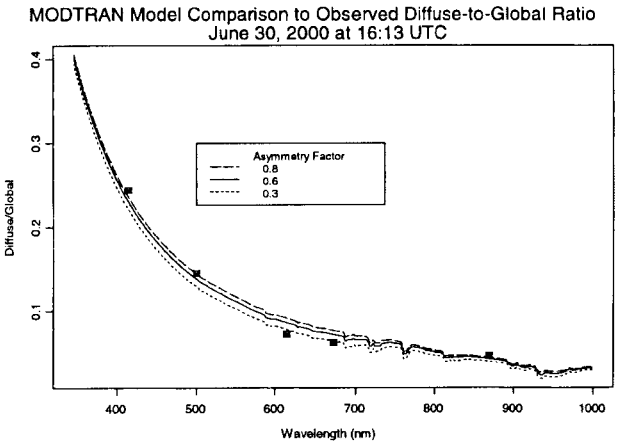

Figure 9. Final MODTRAN model fit to the observed diffuse-to-global ratio.

Nominal Wavelength (nm)	Percent Difference between model and observed transmittance	Percent uncertainty (1 sigma) in measured transmittance (Based on the variability in I_o)
380	4.3%	4.04%
399	2.2	3.30
441	2.7	2.65
521	0.7	2.11
610	2.5	3.97
670	1.0	1.61
782	1.2	1.78
869	0.1	1.15
1030	1.4	1.41

Table 2. Uncertainty comparison between observed transmittance and MODTRAN Model at 11:13 CDT, June 30, 2000.

Table 2 shows that, with one slight exception, the model fits within the 1 sigma error bars of the solar radiometer observations indicating that the reproduction of the atmospheric transmittance is nearly optimal for the data available.

4.2. Step 2: MODTRAN model fit to the observed diffuse-to-global ratio

Once the surface range has been determined in step 1, it is now kept fixed as the procedure moves on to adjust the MODTRAN model to match the observed diffuse-to-global ratio. MODTRAN does not determine the diffuse-to-global ratio directly, but can be calculated using the appropriate output columns in tape 7 when run in the radiance mode.

The approach is to vary the aerosol asymmetry factor (parameter G) for single scattering in MODTRAN 4. It is the controlling parameter in the application of the Henyey –Greenstein aerosol scattering phase function.With the sun high in the sky, the diffuse sky irradiance at the earth's surface is dominated by forward scattering from the atmospheric aerosols. Thus a brighter sky, or higher diffuse-to-global ratio, results when the asymmetry factor is increased. This is seen in Figure 9 that shows the June 30 MODTRAN model calculation of diffuse-to-global ratio using asymmetry factors of 0.3, 0.6 and 0.8 when the solar geometry corresponds to the time of 11:13 CDT (the mean time of the surface reflectance measurements used in the MODTRAN model). It is determined, over the observed spectral range of the shadowband observations, that the best fit is obtained with an asymmetry factor of 0.6. This will be adopted as the value used in the final June 30 MODTRAN model. The asymmetry factor is also a primary parameter that influences sky path radiance. Validation of the MODTRAN Model in predicting sky path radiance will be presented in Section 5.

4.3. Step 3: The top-of -atmosphere radiance prediction

The final step is carried out by setting the altitude and view geometry to that of the down looking sensor and running MODTRAN in the radiance mode. To produce a hypersptectral radiance curve in absolute units the Chance/Kurucz model, that is part of MODTRAN 4.0, is used to supply the solar spectral constant for conversion of the model relative radiance to absolute units.

5. VALIDATION OF THE MODTRAN MODEL

The effectiveness of the above procedure for tuning the MODTRAN model will now be evaluated by comparing the MODTRAN output to in-situ measurements that are independent of those used to constrain the model. Geometries will be set up to have MODTRAN calculate the upwelling radiance from the target surface at ground level and angular resolved sky path radiance, as recorded using the ASD spectroradiometer. For this comparison, the hyperspetral radiance curves will be converted to band-integrated radiance based on the relative spectral response curves for ATLAS bands 1 through 8. Thus, relative uncertainties due to spectral integration will be captured as an error source and will represent typical results for a multispectral imaging system that covers both the VNIR and the SWIR.

5.1. Uncertainty in the ASD radiometer observations

In order to make a meaningful comparison between the model and the ASD measurements of upwelling and sky path radiance, absolute instrumental measurement errors must be established for the ASD spectroradiometer. In addition, the upwelling radiance was recorded with an 8 degree FOV foreoptic and the sky path radiance with a foreoptic having a 1 degree FOV. Thus, converting the raw data to absolute radiance for data sets collected with each foreoptic will have a different gain value and instrumental error. Gains for each spectroradiometer channel were determined using an Optronics integrating sphere with an output certified NIST traceable to 2% and 4% absolute in the VNIR and SWIR.

Measurements errors that included detector noise and drift were evaluated for the ASD by the following procedure. Over a period of 3 weeks (June 2000), spectra of the Optronic integrating sphere, operating of at the fixed calibrated radiance output, were recorded with the ASD FR spectroradiometer. On 11 different days the spectrometer was set outside for an hour to adjust to ambient conditions under illumination from direct sunlight. The instrument was fully powered up and in a normal operational mode. After the hour, the spectrometer was taken into the optics lab and spectra of the integrating sphere were quickly recorded so that the responsivity of the ASD emulated the outside operational conditions. Variations between the recorded spectra in the 11 day data set were used to calculate a band-integrated noise equivalent signal (1 sigma). The resulting gain uncertainties for the ASD with the 1 degree and 8 degree FOV foreoptics are shown in Table 3. They are determined from the root sum square error value for the percent noise equivalent signal for the ASD at the calibrated radiance of the integrating sphere, and from the uncertainty in the sphere's absolute calibration.

ATLAS Channel - FWHM λ	% Uncertainty In Optronics Sphere Absolute Calib.	% Rel. Uncer. ASD Noise Equiv. DN 8-deg. FOV	% Abs. Uncer. In ASD Gain 8-deg. FOV	% Rel. Uncer. ASD Noise Equiv. DN 1-deg. FOV	% Abs Uncer In ASD Gain 1-deg. FOV
1 447-517 nm	2	0.63	2.1	1.83	2.71
2 516-593 nm	2	0.53	2.07	1.55	2.53
3 587-629 nm	2	0.38	2.04	1.14	2.3
4 627-683 nm	2	0.39	2.04	1.21	2.34
5 683-752 nm	2	0.36	2.03	1.22	2.34
6 755-893 nm	2	0.39	2.04	1.5	2.5
7 1536-1797 nm	4	0.35	4.02	1.58	4.3
8 2095-2400 nm	4	1.19	4.17	2.63	4.79

Table 3. Percent absolute uncertainty in ASD spectrometer gain for transforming instrumental digital numbers (DN) to absolute units based on an Optronics sphere calibration. These are band integrated values.

5.2. Comparison of model and measured upwelling radiance

Based on the adopted MODTRAN model for the atmospheric conditions on June 30, 2000, the average upwelling at-surface radiance (ground level) was calculated for a nadir view and the solar geometry that corresponded to the mid-measuremnt of time 11:13 CDT. Figure 10 shows the agreement between the model and observation. In this plot, the ASD measured at-surface radiance is presented based on two absolute calibrations, an ASD factory calibration and the adopted calibration using an Optronics integrating sphere. There was good agreement in the visible and near-IR, however, that is not the case in the SWIR. The discontinuity in the spectrum at 1 micron for the ASD factory calibration indicates a systematic error is present and shows why recalibration with the Optronics sphere was necessary.

The agreement between the model and sphere calibrated observation in this case is excellent. No adjustments were made to the model for this calculation other than setting up the view geometry needed to match the ASD observation. The result is based solely on the model parameter adjustment procedure outlined in Figure 7.

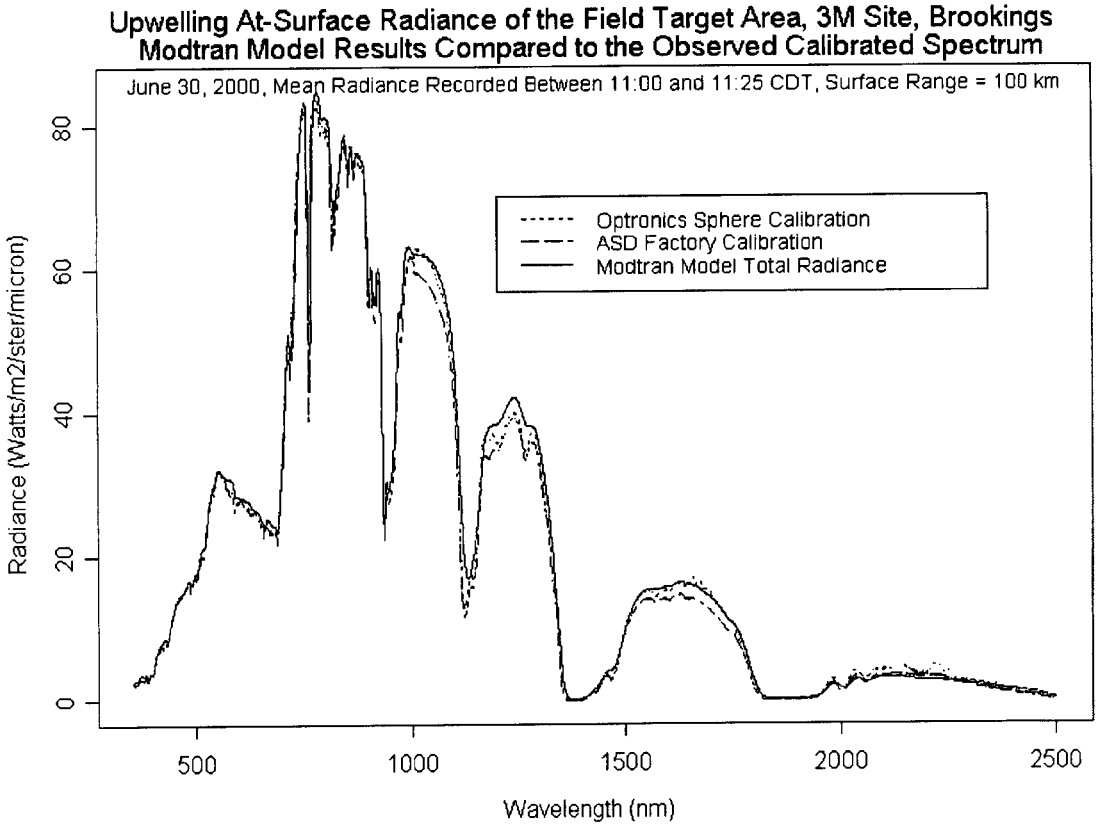

Figure 10. Comparison of the ASD measured and MODTRAN calculated upwelling at-surface radiance

The analysis of the measurement uncertainty in the upwelling radiance coming off the vicarious calibration target, as recorded by the ASD spectroradiometer, is presented in Table 4. The total estimated absolute error in the ASD measurement is derived from the root-sum-square error of the absolute uncertainty in the ASD gain (column 2) and the precision due to instrument noise (column 3) determined by the procedure presented in section 5.1. The difference between the band-integrated radiance from the model and the observation is given in column 9. The result is significant that the difference between the model and the observation is smaller than the measurement error (column 6). Thus the upwelling target radiance predicted by MODTRAN can be interpreted as statistically equivalent to the observation based on the estimated measurement uncertainty.

Atlas Sensor Channel	% absolute uncertainty in ASD gain	ASD noise equivalent signal (DN) (1 sigma)	ASD measured upwelling signal (DN)	% uncertainty due to instrument noise	Total % uncertainty in ASD measurement (1 sigma)	ASD measured radiance W/m^2-ster-micron	MODTRAN model radiance W/m^2 ster micron	% difference between model and observation
1	2.10%	72	1377	5.23%	5.60%	18.9	19.7	4.0%
2	2.07	126	2543	4.95	5.4	28.5	29.4	3
3	2.04	108	2232	4.84	5.3	26.8	27.6	2.7
4	2.04	120	2008	5.98	6.3	25.8	26.4	2.3
5	2.03	125	4059	3.08	3.4	52.9	52.8	0.1
6	2.04	127	5011	2.53	3.3	74.2	74.9	0.8
7	4.02	62	6591	0.94	4.2	14.3	14.3	0
8	4.17	42	3192	1.32	4.4	2.46	3.35	36.2

Table 4. Error analysis of the ASD measured at-surface upwelling radiance spectrum shown in Figure 10 and comparison with MODTRAN model calculations.

5.3. Comparison of ASD measured and MODTRAN calculated sky path radiance radiance

Sky path radiance observations were recorded right after the ground truth reflectance and upwelling radiance of the target surface was measured. The ASD spectroradiometer obtained the observations using foreoptics that consisted of a 1-degree FOV Newtonian telescope fixed to an Alt-Az tracking mount. The pointing accuracy was +/- 0.5° Figure 11 shows the calibrated ASD spectrum of the sky path radiance recorded at 11:28 CDT with the telescope pointed toward an azimuth of 0 degrees (due North) and zenith angle of 70 degrees. The additional curves are MODTRAN generated spectra based on the adopted model derived in section 4 for different aerosol asymmetry factors.

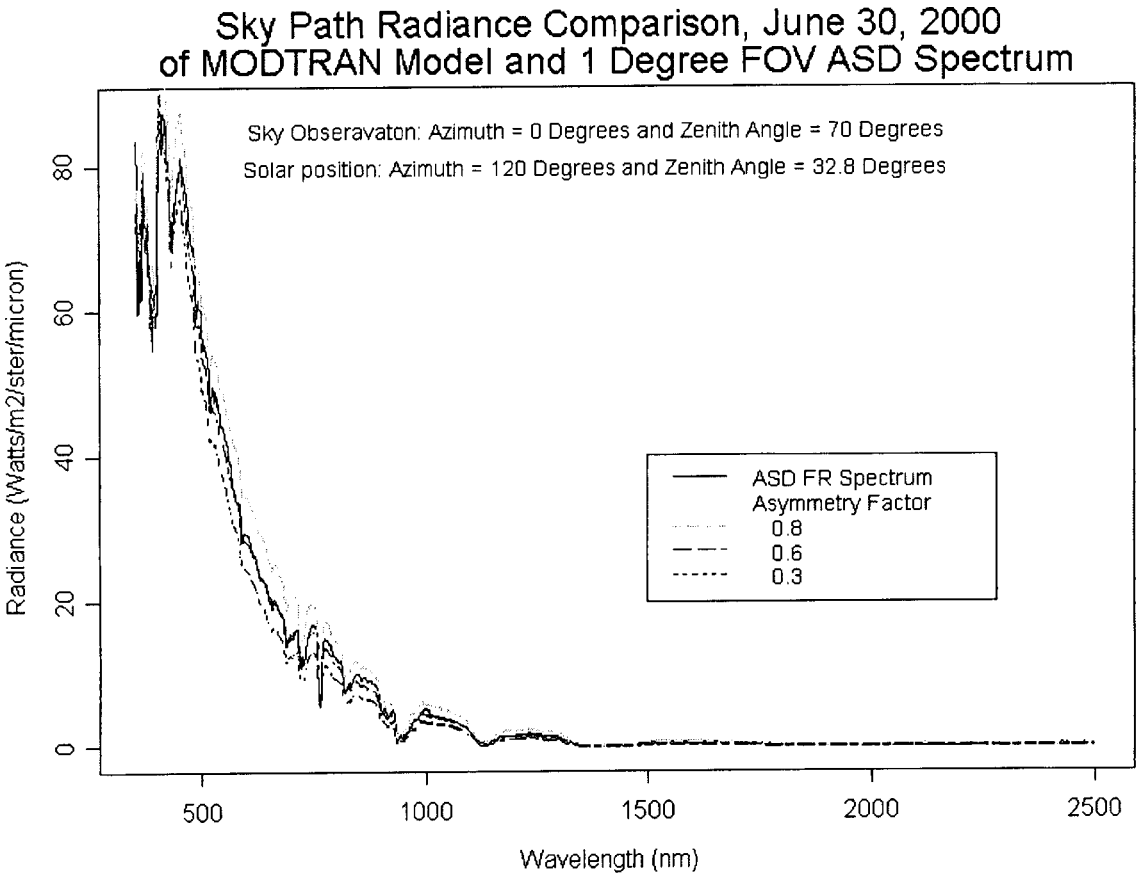

Figure 11. ASD measured and MODTRAN calculated sky path radiance (solar scattering angle of 92 degrees)

The angular direction of the sky path radiance measurement used here was selected as a stressing case for comparison between the model and observation. A 70 degree zenith angle produces a long path length for single scattered photons so that the accuracy of the model extinction will be critical. In addition, the solar scattering angle is near 90 degrees so that polarization effects will have its greatest influence on the ASD measurements and the multiple scattering contribution will be large. The error analysis results are present in Table 5. The MODTRAN emulation was again excellent, recording a difference between the model and observation (column 9) that was smaller than the estimate in the ASD measurement uncertainty (column 6) .

Atlas Sensor Channel	% absolute uncertainty in ASD gain	ASD noise equivalent signal (DN) (1 sigma)	ASD measured sky signal (DN)	% uncertainty due to instrument noise	Total % uncertiatny in ASD measurement (1 sigma)	ASD measured radiance W/m²-ster-micron	MODTRAN model radiance W/m² ster micron	% difference between model and observation
1	2.71	72	5872	1.23	3.0	55.6	54.6	1.67%
2	2.53	126	4623	2.73	3.7	43.6	42.6	2.3
3	2.3	108	3020	3.58	4.3	27.9	27.4	1.7
4	2.34	120	2050	5.85	6.3	20.4	20.1	1.4
5	2.34	125	1341	9.32	9.6	10.49	9.81	6.4
6	2.5	127	744	17.07	17.3	9.40	8.80	6.3
7	4.3	62	403	15.38	16.0	0.155	0.187	20.6
8	4.71	42	27	155.56	155.6	0.049	0.078	59.0

Table 5. Error analysis of the ASD measured sky path radiance spectrum shown in Figure 11 and comparison with MODTRAN model calculations.

To illustrate the success of MODTRAN in reproducing the observed sky path radiance, three MODTRAN models are presented in Figure 11 with asymmetry factors of 0.3, 0.6 and 0.8. This shows that the asymmetry factor of G = 0.6, adopted solely from the measured diffuse-to-global ratio, still provides the best fit. It is felt that since the integrated effects of scattering over the entire sky determining the diffuse-to-global ratio, and the sky path radiance from a narrow 1 degree FOV measurement are both reproduced by the model, that the sky path radiance contribution to the TOA radiance will be accurately modeled also. A quantitative assessment of the predicted TOA radiance accuracy follows.

6. ERROR ANALYSIS OF TOP-OF-ATMOSPHERE RADIANCE

What has been demonstrated in Section 5 is that the MODTRAN model reproduces the ground truth observation of upwelling radiance and sky path radiance within the 1 sigma uncertainties of those observations integrated over the ATLAS spectral response functions. Thus the model provides an excellent representation of the actual atmospheric-target radiative transfer properties at the time the data was collected.

The significant result of the validation in Section 5, in terms of a TOA radiance uncertainty analysis, is that the absolute accuracy of the spectroradiometer radiance measurements are established completely independent of the model characterization. Surface reflectance, transmittance and the diffuse-to-global ratio (the ground truth observations used as MODTRAN inputs for constraining the model) are dimensionless quantities. Thus, the output of MODTRAN in absolute radiance units is defined only by the solar spectral constant applied to the calculations. In contrast, the ground truth measurements of upwelling radiance and sky path radiance are tied to absolute radiance units via laboratory lamp sources. Thus, in principle, the absolute units of the MODTRAN output and spectroradiometer measurements have traceability to national laboratory standards through completely independent paths. The agreement implies that any absolute bias between the instrumental measurements and the MODTRAN model calculation is small[10] and, from here, will be considered negligible in comparison to the magnitude of the instrumental errors derived in section 5.

6.1. **Instrumental based algorithm for estimating TOA uncertainty**

Having demonstrated agreement between the ground-based observations and the radiative transfer calculations with an absolute bias that appears to be negligible, one has an opportunity to conduct a TOA radiance error analysis based on the instrumental measurement errors which will have some advantages over a model parameter sensitivity analysis. A root-sum-squared (RSS) analysis of model input parameter errors may not capture all error contributions. This leads one to consider the following questions. Are atmospheric parameters that are assumed and not measured producing unknown bias errors? What is the magnitude of the correlation errors between model parameters? What is the contribution of algorithm errors in modeling the physics involved? Are error contributions due to parameter temporal variability and non-uniformity realistically assessed? Basically, one wonders how accurate an error estimate really is, based on a

radiative transfer model that may not fully capture the actual radiometric processes occurring in the atmosphere and terrain imaged by the sensor, especially at a site that is not an ideal calibration target.

The attempt here is to avoid these questions about unknown and unexplored uncertainties in the model calculations by recognizing that they do not apply to the measurement errors of the radiometer observations. Thus, if the ground based measurement errors from the solar radiometer and the spectroradiometer observations can be utilized in a way to determine the uncertainty in the top-of-atmosphere radiance, then the model dependent errors are bypassed. This would result in an alternate approach to a TOA radiance error investigation that is more in tune with the actual environment under which a vicarious calibration is carried out. An instrument based error analysis that attempts to produce this result with minimal dependence on model error sources is described next.

The top-of-atmosphere target radiance, L_s^{TOA}, as seen by an orbiting sensor, can be expressed as three components using the transfer equation

$$L_s^{TOA} = L_t^{up} T_{sen} + L_p^{TOA}. \quad (1)$$

Here L_t^{up} is the upwelling target radiance at ground level, T_{sen} is the transmittance along the path between the target and the sensor and L_p^{TOA} is the sky path radiance contribution as seen from the sensor when viewing the target (the signal produced if looking at a surface of zero reflectance). Because the terms in (1) are going to be linked directly to the ground measurements, in which their uncertainties are determined by the physics of the measurement process rather then environmental phenomena, they are assumed to be independent (i.e., uncorrelated) variables. Thus the error propagation equation estimating the TOA radiance uncertainty, $\sigma_{L_s^{TOA}}$, can be written as:

$$\sigma_{L_s^{TOA}} = \left[\left(T_{Sens} \sigma_{L_t^{up}} \right)^2 + \left(L_t^{up} \sigma_{T_{sens}} \right)^2 + \left(\sigma_{L_p^{TOA}} \right)^2 \right]^{1/2} \quad (2)$$

How these at-sensor quantities are defined in terms of the ground measurements and the MODTRAN calculations are presented as follows.

The upwelling target radiance measured at the ground, $L_{t,meas}^{up}$, is estimated by the MODTRAN model, $L_{t,Mod}^{up}$, in its tape 7 output (GRND RFLT/TOT TRANS) when run to calculate the TOA radiance for a downlooking sensor. Thus, if MODTRAN has been properly constrained by the ground-truth data, it should be true that $L_{t,meas}^{up} = L_{t,Mod}^{up}$ within the uncertainty of the ground measurement. Since this has been demonstrated in Section 5 that they are statistically equivalent, it can be specified that $L_t^{up} = L_{t,meas}^{up} = L_{t,Mod}^{up}$ with an estimated uncertainty $\sigma_{L_t^{up}} = \sigma_{L_{t,meas}^{up}}$. The uncertainty values are located in column 6 of Table 4.

At wavelengths for which the extinction law applies, $T = e^{-km}$, transmittance follows the principle of reversibility. Therefore measurements along the path from the ground toward the sun, $T_{sun,meas}$, provides the transmittance from the sensor to the ground, T_{sen}, after including an air mass (m = sec z) correction due to different zenith angles (z). Since it was shown that the MODTRAN model transmittance at the solar zenith angle, $T_{sun,Mod}$, equaled the solar radiometer measured transmittance, $T_{sun,meas}$, within the measurement uncertainty, $\sigma_{T_{sun,meas}}$, under stable sky conditions it can be specified that:

$$T_{sen} = T_{sen,Mod} = \left(T_{sun,meas} \right)^{(m_{sen}/m_{sun})} = \left(T_{sun,Mod} \right)^{(m_{sen}/m_{sun})}.$$

Taking the derivative with respect to transmittance, the relation for the sensor to ground transmittance uncertainty, $\sigma_{T_{sens}}$, in terms of the solar radiometer measured ground to sun uncertainty, $\sigma_{T_{sun,meas}}$, can be expressed as:

$$\sigma_{T_{sens}} = \sigma_{T_{sun,meas}}\left[\left(m_{sen}/m_{sun}\right)\left(T_{sun,Mod}\right)^{(m_{sen}/m_{sun}-1)}\right] = \sigma_{T_{sun,meas}}\left[\left(m_{sen}/m_{sun}\right)\frac{T_{sen,Mod}}{T_{sun.Mod}}\right].$$

In order to estimate the transmittance in the orbiting sensor observation, $\sigma_{T_{sens}}$, an additional error source must be accounted for here because the transmittance observations are recorded at only a few wavelengths by the solar radiometer. The transmittance measurements are not hyperspectral as are the radiance measurements. Thus, the uncertainty, $\sigma_{T_{sun,meas}}$, at the nominal wavelength of the ATLAS sensor bands, is estimated from the uncertainty recorded at the nominal wavelengths of the solar radiometer (column 3 of Table 2) by linear interpolation. Since the interpolation process results in additional uncertainty, an additional 0.5% of the total transmittance, $0.005T_{sen,Mod}$, will be combined with $\sigma_{T_{sun,meas}}$ as a root-sum-square error contribution. This is estimated from the magnitude of the wavelength dependent variations in the transmittance uncertainty.

The determination of the sky path radiance as seen by the sensor is the most difficult of the three to estimate from ground observations. However, good results can be obtained by recording the sky path radiance from the ground as close as possible to the same solar scattering angle seen by the down looking sensor. This will typically fall into the realm of backscattering and the application of the Henyey –Greenstein phase function in MODTRAN works well here. When compared to actual sky path radiance observations, MODTRAN can reproduce those backscatter observations with nearly constant bias for large solar scattering angles (> 60 degrees). This means that if MODTRAN can be set up to reproduce the ground-based measured sky path radiance at one scattering angle, then a sky path radiance difference, $\Delta L_{p,Mod} = L^{TOA}_{p,Mod} - L^{ground}_{p,Mod}$, relative to the scattering angle of the downlooking sensor calculated using the same MODTRAN model, can be added to the observed sky path radiance introducing only a relative error. Here the relative error contribution is adopted as $\sigma_{\Delta L_{p,Mod}} = 0.03L^{TOA}_{p,Mod}$. The +/- 3% value is assessed from a MODTRAN analyses of constant zenith angle (i.e. almucantar) spectroradiometer scans of the sky in the VNIR[11]. The relation between the ground-based sky path radiance observation, $L^{ground}_{p,meas}$, and the TOA at-sensor sky path radiance, L^{TOA}_{p}, can now be written as:

$$L^{TOA}_{p} = L^{ground}_{p,meas} + (L^{TOA}_{p,Mod} - L^{ground}_{p,Mod}) = L^{ground}_{p,meas} + \Delta L_{p,Mod}.$$

Since it has been demonstrated statistically that $L^{ground}_{p,meas} = L^{ground}_{p,Mod}$ it can be expressed that:

$$L^{TOA}_{p} = L^{TOA}_{p,Mod} \text{ and } \left(\sigma_{L^{TOA}_{p}}\right)^2 = \left(\sigma_{L^{ground}_{p,meas}}\right)^2 + \left(\sigma_{\Delta L_{p,Mod}}\right)^2 = \left(\sigma_{L^{ground}_{p,meas}}\right)^2 + \left(0.03L^{TOA}_{p,Mod}\right)^2.$$

Returning to equation (2), the results of this section can be inserted to give the final expression for the estimate in the TOA radiance uncertainty as defined by the measurement uncertainties of the radiometers validating the MODTRAN calculated transmittance, upwelling radiance, and sky path radiance components of equation (1) . The final error propagation equation for estimating the uncertainty in the MODTRAN calculated TOA radiance is:

$$\sigma_{L^{TOA}_{s}} = \left[\left(T_{Sens,Mod}\sigma_{L^{up}_{t,meas}}\right)^2 + \left(L^{up}_{t,Mod}\left[\left(m_{sen}/m_{sun}\right)\frac{T_{sen,Mod}}{T_{sun.Mod}}\right]\right)^2\left(\sigma_{T_{sun,meas}}{}^2 + (0.005T_{sun,Mod})^2\right) + \left(\sigma_{L^{ground}_{p,meas}}\right)^2 + \left(0.03L^{TOA}_{p,Mod}\right)^2\right]^{1/2} \quad (3)$$

6.2. Top-of atmosphere band-integrated radiance uncertainty estimates for the June 30, 2000 MODTRAN model
For the MODTRAN Model of June 30, 2000, constrained by in-situ measurements via procedures presented in section 4 and verified by ground-based radiometer measurements in section 5, the uncertainty in the TOA radiance prediction can be estimated using equation (3). All of the inputs to (3) have been band-integrated based on the relative spectral responses for ATLAS channels 1 to 8 from the model output set up for a nadir view. These are presented in Table 6 along with the results for equation (3) in the last two columns. The outcome shows that at least for this one vicarious calibration field campaign, in Brookings, South Dakota, reflectance-based TOA radiance predictions have been effectively estimated to be between 3% and 5% in the solar reflective spectrum from 0.4 to 1.6 microns. In the short wave visible spectrum the uncertainty is dominated by the sky path radiance uncertainty. In the longwave visible, the uncertainty in all three components of equation (1) play balanced roles. In the NIR and the SWIR the dominant uncertainty is in the measurement of upwelling radiance. The much larger uncertainty for channel 8 (2.1 to 2.4 microns FWHM) was traced to problems with the integrating sphere calibration of the ASD and, of course, the lower solar irradiance signal.

ATLAS Channel	Total TOA Radiance (Watts/m^2-ster-micron)	At-Surface Radiance, (Watts/m^2-ster)	At-Surface % Relative Uncertainty	At-Surface Radiance Uncertainty	Transmittance to Sensor	Transmittance % Relative Uncertainty	Transmittance Uncertainty,	Transmittance to Sun	Sky Path Radiance, L_p (Watts/m^2-ster-micron)	Sky Path Radiance % Relative Uncertainty	Sky Path Radiance Uncertainty, (Watts/m^2-ster-micron)	Total TOA Radiance Uncertainty, (Watts/m^2-ster-micron)	Total TOA Radiance % Estimated Uncertainty
	L_s^{TOA}	$L_{t,Mod}^{up}$		$\sigma_{L_{t,meas}^{up}}$	$T_{sen,Mod}$		$\sigma_{T_{sun,meas}}$	$T_{sun,Mod}$	$L_{p,Mod}^{TOA}$		$\sigma_{L_{p,meas}^{ground}}$	$\sigma_{L_s^{TOA}}$	
1	45.16	19.85	5.64	1.12	0.811	2.30	0.019	0.773	29.07	3.0	0.866	1.53	3.4
2	41.94	29.43	5.37	1.58	0.840	3	0.025	0.808	17.21	3.7	0.64	1.56	3.7
3	35.44	27.57	5.25	1.45	0.862	3.8	0.033	0.833	11.68	4.3	0.498	1.39	3.9
4	32.15	26.56	6.32	1.68	0.883	2.8	0.025	0.858	8.7	6.3	0.548	1.6	5.0
5	54.2	54.72	3.69	2.02	0.868	1.7	0.015	0.841	6.7	9.6	0.644	1.88	3.5
6	74.12	77.03	3.25	2.5	0.903	1.5	0.014	0.883	4.55	17.3	0.785	2.39	3.2
7	14.04	14.71	4.13	0.61	0.945	1.8	0.017	0.933	0.14	16.0	0.022	0.58	4.1
8	2.35	2.36	4.37	0.1	0.917	2.8	0.026	0.899	0.19	155.6	0.296	0.31	13.2

Table 6. Inputs and results for the analysis of the TOA radiance uncertainty using the error propagation model presented by equation (3)

7. APPLICATION TO IKONOS VICARIOUS CALIBRATION

The field campaign at Brookings was part of a NASA sponsored effort to evaluate the absolute IKONOS multispectral imagery radiometry in conjunction with similar efforts carried out by teams from NASA Stennis Space Center and the University of Arizona[12]. The sites characterized by these groups in June of 2000 included dry lake playas at Railroad Valley and Lunar Lake, Nevada, and White Sands Missile Range, New Mexico. A comparison of the Brookings vicarious calibration results with these others provides an opportunity to determine consistency with the error assessment presented in this paper relative to their independent determinations of the TOA radiance. Using the average surface reflectance spectrum recorded between 11:49 and 12:10 CDT (Fig. 3), the MODTRAN model outlined in this paper was used to generate a TOA spectrum for the IKONOS overpass at 12:13 CDT. TOA radiance uncertainties were assessed by equation (3) for the four IKONOS multispectral bands and came out essentially the same as those obtained for ATLAS channels 1, 2, 4, and 6 presented in Table 6.

The MODTRAN predicted in-band radiance for Brookings and the other sites are plotted verses average target digital numbers (DN) obtained from IKONOS images in each of the four multi-spectral bands. With each measurement equally

weighted, a straight line fit was performed to generate a composite estimate for the sensor gain. There was no evidence of a sensor bias (Space Imaging routinely measures and subtracts out the bias) so the offset was set to zero for the least squares fit. In this result, the error of this composite measurement should be smaller than the error in each individual measurement. Thus, the uncertainties in the Brookings points should contain the fitted line if the error procedure presented in this paper has assessed the absolute errors correctly.

Two points are plotted for the Brookings gain values in Figure 12 that include the grass calibration target and also targets determined to have zero reflectance. These would be locations of deep shadows produced by tree lines in the blue and green bands, and water bodies in the red and near-IR bands. A zero reflectance TOA radiance will have an error bar determined by the sky path radiance uncertainty (column 11 in Table 6). Because of the large range in reflectance of the various calibration sites, the gain estimates cover most of the dynamic rang of the sensor. The reflectance of the Brookings target is relatively low and will fall in the low radiance end of the plot. Because of the large radiance scale the error bars are small in the figure but reflect the result that the predicted TOA radiances show excellent agreement relative to the 1 sigma uncertainties of the single gain fit of all the vicarious measurements in each band. The result supports the conclusion that the accuracy assessment presented in this investigation captures the significant random and systematic errors influencing the prediction of the TOA radiance.

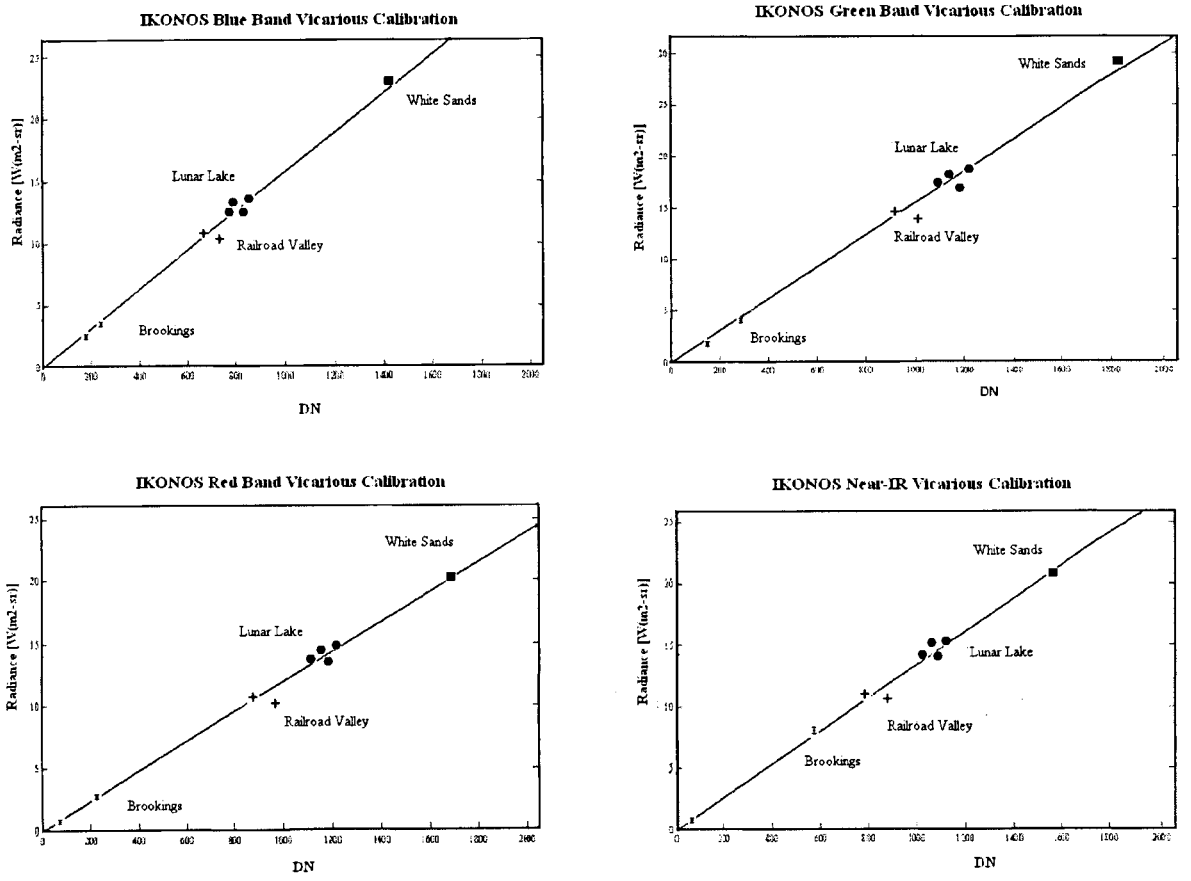

Figure 12. Single gain fit to the summer 2000 vicarious calibration results for IKONOS. The Brookings results for June 30. 2000 fits the unweighted least-squares regression line within the 1 sigma uncertainty error bars for all four multispectral bands.

8. CONCLUSION

As the need for higher accuracy grows, remote sensing data mandates improvements in the way data quality is presented to the remote sensing community. The reflectance-based method of vicarious calibration is a widely used technique for

assessing and trending the calibration performance of remote sensing systems on orbit. The application of this assessment, however, is incomplete unless it also provides an estimate of the absolute uncertainty. A methodology for estimating the TOA radiance and setting limits on the knowledge of the radiance accuracy have been demonstrated in this paper. In summary, once it has been confirmed that radiative transfer model calculations agree within the uncertainties of ground-based measurements relative to each of the parameters in equation (1), an estimate of the TOA radiance uncertainty, that is sensitive to all potential error sources, can be derived by equation (3). MODTRAN is used to calculate the TOA radiance uncertainties based on those of the calibrated radiometer measurements used to validate the model performance at the time of the sensor overpass. Based on the test case applied here for ATLAS and IKONOS, multispectral band integrated TOA radiances where verified to the 3% to 5% level. The results of this investigation show that less ideal target sites, such as located in the Northern Great Plains, can be effectively used for the vicarious calibration of orbiting sensors if the set of field measurements and procedures outlined here are applied.

References

1. P.N. Slater, S.F. Biggar, R.G. Holm, R.D. Jackson, Y. Mao, M.S. Moran, J.M. Palmer, B. Yuan, "Reflectance- and Radiance-Based Methods for the In-Flight Absolute Calibration of Multispectral Sensors," Remote Sensing of the Environment, Vol. 22, pp. 11-37, 1987.

2. P.N. Slater, S.F. Biggar, K.J. Thome, D.I. Gellman, and P.R. Spyak, "Vicarious Radiometric Calibration of EOS Sensors, Journal of Atmospheric and Oceanic Technology, Vol. 13, pp.349-359, 1996.

3. K.J. Thome, "Absolute Radiometric Calibration of Landsat-7 ETM+ using the Reflectance-based Method," Remote Sensing of the Environment, Vol. 78, pp. 27-38, 2001.

4. K.P. Scott, K.J. Thome, and M.R. Brownlee, "Evaluation of the Railroad Valley for use in vicarious calibration," Proc. SPIE, Vol. 2818, 1996.

5. S.F. Biggar, P.N. Slater, and D.I. Gellman, "Uncertainties in the In-Flight Calibration of Sensors with Reference to measured Ground Sites in the 0.4 to 1.1 μm Range." Remote Sensing of the Environment, Vol. 48, pp. 245-252, 1994.

6. P.N. Slater, S.F. Biggar, J.M. Palmer, and K.J. Thome, "Unified approach to pre- and in-flight satellite-sensor absolute Radiometric Calibration", SPIE, Vol 2583, pp. 130-141, 1995.

7. D. Magdeleine, and P.N. Slater, "Calibration of Space-Multispectral Imaging Sensors: A Review," Remote Sensing of the Environment, Vol. 68, pp. 194-205, 1999.

8. K.J. Thome, "Ground-Look Radiometric Calibration Approaches For Remote Sensing Imagers In The Solar Reflective", Pecora 15/ Land Satellite Information IV Conference, Proc. ISPRS Vol 34, part 1, 2002.

9. A. Burk, G.P. Anderson, P.K. Acharya, J.H. Chetwynd, L.S. Bernstein, E.P. Shettle, M.W. Matthew, and S.M. Adler-Golden, MODTRAN 4 Users Manual, Air Force Research Laboratory, Space Vehicles Directorate, Air Force Material Command, Hanscom AFB, Massachusetts. 1999.

10. D.B. Pollock, T.L. Murdock, R.U. Datla, and A. Thompson, "Data uncertainty traced to SI units, Results reported in the International System of Units," Int. J. Remote Sensing, Vol. 24, pp. 225-235, 2003.

11. S.J. Schiller, and J. Luvall, "Evaluation of the Aerosol Scattering Phase Function from PGAMS Observations of Sky Path Radiance", in the proceedings of *IGARSS96: Remote Sensing for a Sustainable Future*, Lincoln, Nebraska, pp.1286-89, 1996.

12. M. Pagnutti, R.E. Ryan, M. Kelly, K. Holekamp, V. Zanoni, K. Thome, S.J. Schiller, "Radiometric Characterization of IKONOS Multispectral Imagery", Submitted to Remote Sensing of the Environment, 2003.